Robotizing Double-Electrode GMAW Process through Learning from Human Welders

Rui Yu[1], Yue Cao[1], Jennifer Martin[2], Otto Chiang[2], and YuMing Zhang[1*]

1: Department of Electrical and Computer Engineering and Institute for Sustainable Manufacturing, University of Kentucky, Lexington, KY 40506, USA
2: Toyota Motor North America, USA.
*: Corresponding author/ email: yuming.zhang@uky.edu

Abstract: Gas metal arc welding (GMAW) is the most robotized arc welding process and most widely used process for wire arc additive manufacturing (WAAM). Double-electrode GMAW (DE-GMAW) is its novel modification achieved by adding a second/bypass electrode. It provides the capability to freely adjust the base metal current (heat input) without changing the wire current (mass input). However, it must be robotized in order to be adaptive to manufacturing variations and constraints. Due to the complexity of the process, we propose learning from human welders through their attempts to adjust the bypass electrode in collaboration with the robotized GMAW. To generalize human success using a follower robot/ surrogate, the distance between the wire and bypass electrode is proposed as the process state to quantify human observation and operation. As such, Inertial Measurement Unit (IMU) sensors are integrated to track the wire and bypass electrode operated by both the lead robot and the human welder. To interpret human adjustments per arc observation, a Convolutional Neural Network (CNN) is employed to process arc images and calculate the distance. The automatically obtained distance labels from IMU signals are used to train the CNN; however, they are noisy and inaccurate. Thus, the CNN is finely tuned through transfer learning using manually labeled distances. With accurately automatically calculated distances from the finely tuned CNN for all the data, the demonstrations from human welders are analyzed. The generalized knowledge is implemented by a robotic surrogate, substituting for the human welder to fully automate the DE-GMAW. Experiments demonstrated the superior performance of the fully robotized, and adaptively controlled, DE-GMAW process.

1. Introduction

Gas metal arc welding (GMAW) is a welding process that uses an electric arc formed between a consumable electrode wire and the workpiece to create a weld joint. The consumable electrode wire is typically made of the same material as the workpiece or a compatible material [1]. It serves as both the electrode and filler material. As the wire is fed into the arc, it melts and becomes part of the weld pool. GMAW is of high productivity as its electrode/wire is continuously fed and effectively melted by the arc. It is thus economically favorable and has been more robotized compared with other welding techniques such as gas tungsten arc welding (GTAW) [2, 3]. Due to its high deposition rate, GMAW is particularly well-suited for efficiently fabricating extensive, large-scale structural metal components. It

has been employed for wire arc additive manufacturing (WAAM) [4-20], also known as welding-based rapid prototyping [21, 22].

As the electrical current flows through the fed wire toward the base metal, a high-energy electric arc is created between the consumable wire and the workpiece. This arc generates intense heat to finish the melting process. This heat is a crucial component of the welding process, as it causes the consumable wire and the base metal to melt and fuse together, creating the weld joint. However, a consequence of this heat generation is that not only does the arc generate heat on the consumable wire, but it also imparts heat to the base metal (workpiece). This phenomenon introduces the potential for excessive heat accumulation within the workpiece during the welding process. As the heat accumulates, the temperature of the workpiece can rise, leading to distortion and warping of the material [23, 24], which is particularly critical for WAAM.

Innovations have been made to reduce/control the heat on the base metal without compromising the melting of the wire. Proposed methods include but not limited to AC GMAW [25] which alternates the arc polarity on the wire and base metal, controlled short-circuiting process [26] including the cold metal transfer (CMT) which retracts the fed wire to re-ignite the arc, and ice welding [27] where a cold wire is added to the weld pool. An impactful solution to address this issue was proposed/developed at the University of Kentucky through the utilization of the double-electrode gas metal arc welding (DE-GMAW) process [28]. A non-consumable GTAW bypass torch was added on the side of the main GMAW torch to decouple the current from the wire into base current and bypass current. This allows increasing the wire-related melting current while maintaining desired level of base metal current. Follow-up efforts also replaced the non-consumable GTAW torch by a consumable GMAW torch [29]. Yang built thin-walled parts with this DE-GMAW process [30]. By analyzing the mean bead width and deposition height, experiments proved that under a given deposition rate, as the bypass current increased, the width of the deposited part reduced, while the height exhibited a proportional increase. Xue extended this process by introducing another GTAW power to transform the DE-GMAW system into a Dual-GMAW system [31]. By incorporating two bypass torches, positioned on the left and right sides of the main torch, three current loops were established: left bypass, right bypass, and main current. Such system reduces the heat input to a minimum level.

All the existing experiments used a pre-fixed relationship between the main torch and the bypass torch. The placement of the bypass electrodes in relation to the main electrodes is established before the welding starts. Implying a lack of flexibility or adaptability to adjust this process, pre-fixed relationship makes it impossible for complex structures that are common in welding manufacturing and WAAM. Therefore, it has a need to robotize this DE-GMAW process. To this end, the two torches need to be handled by two separate operators, called as lead torch/main torch and follower torch/bypass torch. The follower should have the ability to adaptively position the second electrode at the optimal position to sustain the bypass arc. Since DE-GMAW has never been robotized before, it's hard to decide how to perform the welding process with the robot from scratch. Human welders can quickly learn and improve their welding skill with several attempts. In [32, 33], their responses to weld pool surface in gas tungsten arc welding (GTAW) have been successfully learned to adjust the welding speed to control the weld

penetration. The learned human response model has also been used to robotize GTAW process [34]. Thus, this work proposes to learn the control methodology from skilled human welders and then generalize their expertise to establish an automatic system which contains a robot and a tractor equipped with multiple sensors to execute the DE-GMAW process.

2. Proposed Approach and Arc Image Inspection

2.1 Proposed Approach

We purposely conducted the DE-GMAW process under various conditions [35]. This earlier study revealed three operating modes of the DE-GMAW process, as shown in Figure 1: (a) open arc/simple arc (SA), which is essentially the conventional GMAW process with the presence of the (non-functioning) bypass electrode; (b) parallel arc, where a secondary arc is established between the bypass electrode and the wire, alongside the main gas metal arc; and (c) serial arc, in which the second arc bridges the bypass electrode and the workpiece. The parallel arc mode is the desired state, as it delivers the targeted benefits. It is critical to assure that the process operates in the desired parallel arc mode as the simple arc mode does not reduce the heat input as intended from the conventional GMAW and the serial arc model evens increases.

To facilitate real-time process monitoring, we developed a deep learning model capable of directly detecting the operating mode from arc images. However, for effective control of the process in the desired mode through learning from human welders, it's necessary to quantify the operations of human welders. Moreover, beyond mere classification, it's important to quantify the distinct arc behaviors.

Given that human welders do not typically control the DE-GMAW process under the single arc mode, we seek for a method to quantify the arc behaviors specifically during the parallel and serial arc modes. A close examination of pertinent arc images reveals a strong correlation between arc behaviors/arc modes and the distance separating the bypass electrode and the wire tip. To validate this hypothesis, it is possible to compute the statistical measures of this distance across various modes and subsequently compare these statistics among the different modes. Such an analysis would serve to confirm the utility of this distance as a quantifiable parameter for mode characterization.

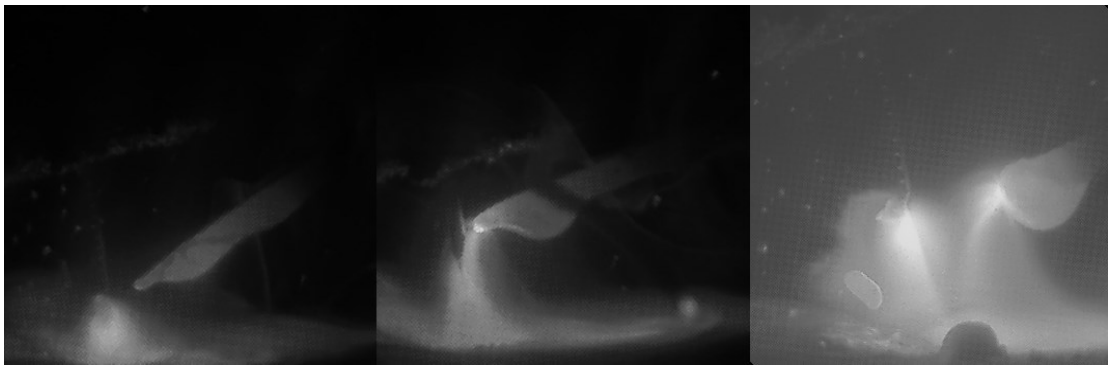

(a) Single arc (b) Parallel arc (c) Serial arc

Figure 1 Three distinct modes during DE-GMAW system operation.

One challenge that impacts our ability to validate the efficacy of the distance lies in the effective calculation of this distance itself. While conventional machine vision algorithms can be developed for this purpose, the endeavor of creating and validating an efficient algorithm is time-consuming. It necessitates an in-depth comprehension and analysis of complex arc images, along with their features under various conditions. In this context, deep learning emerges as a more effective approach for calculating this distance. It avoids the need for time-consuming human-dependent understanding and analysis.

Training a deep learning model to calculate the distance from arc images requires an exceptional number of arc images labeled with their respective distances. Manually labeling a large quantity of arc images is impractical, while achieving precise automatic labeling through image processing presents the same challenge we are trying to address. Consequently, we propose the installation of miniature IMU (inertial measurement unit) sensors on the tractor that carries the GMAW torch, holding the wire, as well as on the human held GTAW torch/bypass electrode. Since the IMU sensor and bypass electrode exhibit a different geometric correlation each time the welder grips the torch, we will introduce a simple yet effective method to adaptively calibrate it. In this way, we will be able to automatically obtain the needed large number of distance labels to train a deep learning model to calculate the distance from the arc image. However, analysis shows that the precision needed to quantify the state using the distance is high. To further improve the calculation accuracy for the distance, we will use transfer leaning for fine training the deep learning model using manually labeled arc images of relatively small quantity.

As such, we propose the following research path: (1) Examining the arc images in different states to see if the distance varies with the state. However, as we are unable to measure the distance yet, such examination is just to hypothesize the correlation between the state and distance. We will then propose a formal definition for the distance. (2) Developing an experimental system that allows us to automatically obtain the distance although such distance may not be as accurate as desired. (3) Training a deep learning model using the IMU sensors based automatically obtained labels and then refine the training using manually labeled arc images. We are now able to accurately calculate the distance. (4) All the arc images can be classified into three different state modes. The arc images in the same mode can be used to calculate the distances. We will verify the effectiveness of the distance for its capability in determining the state modes. (5) We will then study the statistics of the distance on different state mode and find the desired distance for the robotized system to real-time adjust the bypass electrode.

2.2 Analysis of Arc Images

Figure 2(a) depicts various arc images classified under the parallel arc mode. Despite the differences in details, they share a common characteristic: a bright region bridging between the electrode and the wire. This region corresponds to the ionized gas forming the arc column between the electrode and wire – the bypass arc through which a portion of the current flows from the wire to the bypass electrode, which would otherwise go to the workpiece. Moving to Figure 2(b), we observe images classified under the serial arc mode. Again, despite differences, they share a common attribute: the absence of a bright region bridging the bypass electrode and the wire, but instead with the workpiece. Here, all the current flows

from the wire to the workpiece (as in conventional GMAW) and additionally the portion provided by the GTAW power source further flows from the workpiece to the bypass electrode, accompanied by a respective bright region between the workpiece and the bypass electrode. In Figure 2(c), bright regions exist between the wire and bypass electrode, as well as between the workpiece and bypass electrode in each arc image. This blend of parallel and serial modes suggests that the classification into three modes is mostly for convenience and may be considered somewhat artificial. Introducing a more accurate description for the process state could provide a more nuanced feedback of the process.

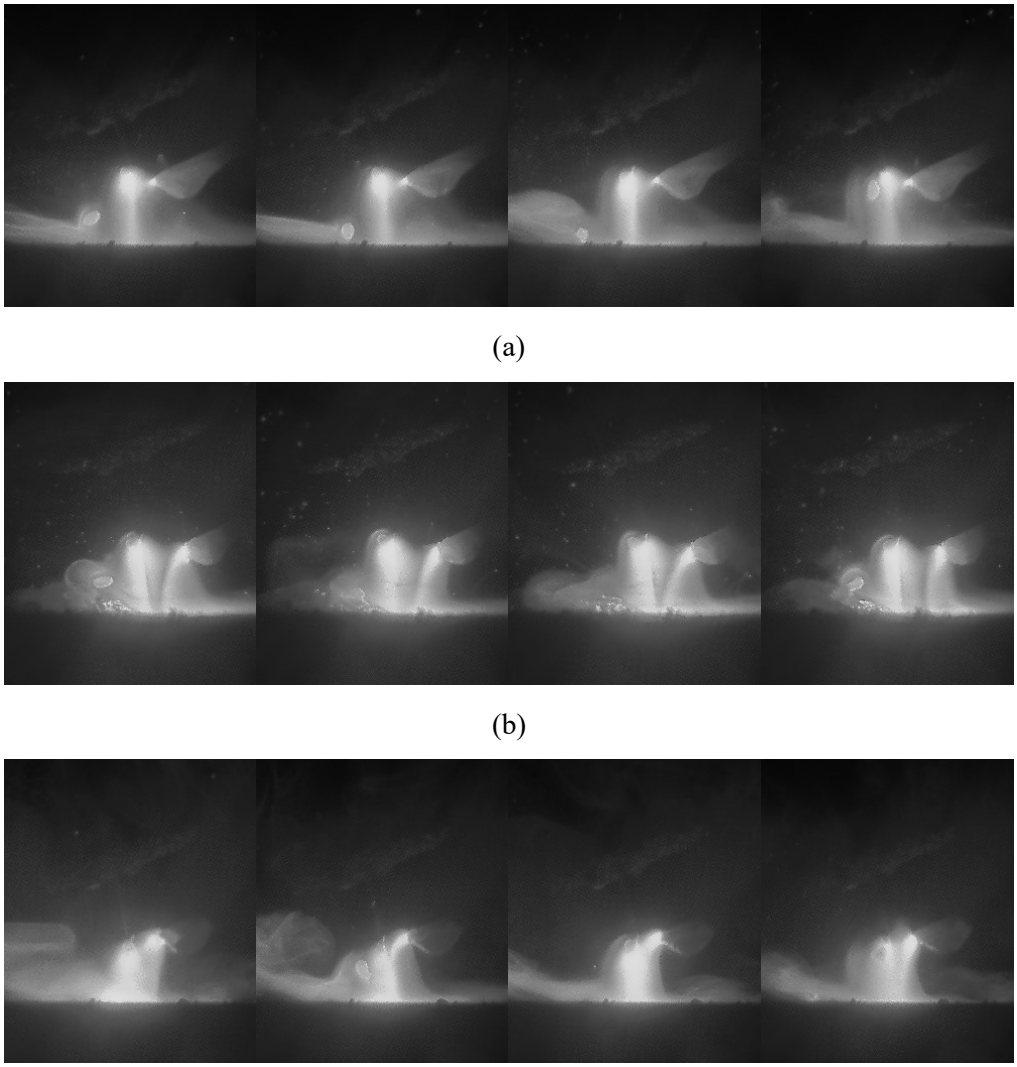

(a)

(b)

(c)

Figure 2 Classified arc images. (a) Classified to parallel arc; (b) Classified to serial arc; (c) Incorrectly classified arc images.

Observing the arc images in Figure 2 clearly suggests that the distance between the wire and bypass electrode in (a) is shorter than that in (b). Additionally, the average distance in (c) is shorter than that in (b), but longer than in (a). Consequently, if distances are utilized, the arc images could be quantitatively described, capturing both the subtle quantitative differences within a mode and the significant qualitative differences among different modes. The operation of the human welder can also be

quantified by using the distance as a single state. As such, we tentatively propose using the distance to study human welder operation.

3 Human Movement Sensing

Figure 3 shows the experimental system developed to learn from human welder. In this system, the tractor carries the GMAW torch/wire to move while the human welder carries the GTAW torch/bypass electrode to follow the wire. The arc images shown in Figure 1 are captured by a camera, Point Grey camera FL3-FW-03S1C, at 60 frames per second. Both the tractor and the welding torch are installed with an IMU sensor, Intel RealSense T265, so that their movement can be monitored.

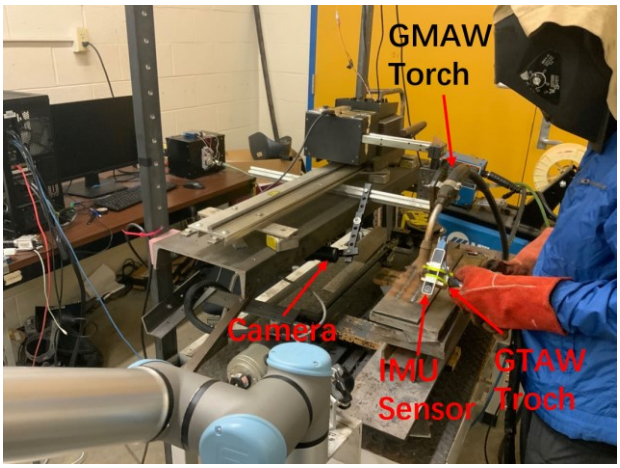

Figure 3 Experimental system designed to learn from human welder.

In typical welding operations, welders closely observe the weld pool to effectively respond to the welding process. In the case of DE-GMAW, welders focus on monitoring the behavior of the arc in order to make precise adjustments to the position of the bypass electrode. The arc images depicted in Figure 1 and Figure 2 serve as the input, while the corresponding operation of the bypass electrode via the GTAW torch represents the welder's output. While the welder's input is captured and recorded by the camera, the output is documented by the IMU sensor integrated into the welding torch. The IMU sensor detects movements within its coordinate system with respect to the world coordinate system. In our specific application, we require the movement data of two specific endpoints: the wire tip from the IMU sensor installed on the tractor and the bypass electrode tip from the IMU sensor installed on the torch.

The challenge in translating the IMU sensor data to the endpoint data position primarily arises from the bypass electrode. This is due to the fact that the correlation between the IMU sensor's coordinate system and the endpoint shifts every time the welder replaces the tungsten electrode in the GTAW torch. In contrast, this issue does not occur with the IMU and wire tip data correlation, as it remains constant.

The correlation between the endpoint's position of the bypass electrode, denoted as P_{end}, and the IMU sensor is given through the equation:

$$P_{end} = R * V + T \tag{1}$$

where V is the vector responsible for translating from the sensor's coordinate system to the bypass electrode's endpoint, and (T, R) are obtained from the real-time data output of the sensor. Specifically, T represents the 3D coordinates, and R symbolizes the rotation matrix derived from quaternions (q_w, q_x, q_y, q_z):

$$R = \begin{bmatrix} 1 - 2 * {q_y}^2 - 2 * {q_z}^2 & 2 * q_x * q_y - 2 * q_z * q_w & 2 * q_x * q_z + 2 * q_y * q_w \\ 2 * q_x * q_y + 2 * q_z * q_w & 1 - 2 * {q_x}^2 - 2 * {q_z}^2 & 2 * q_y * q_z - 2 * q_x * q_w \\ 2 * q_x * q_z - 2 * q_y * q_w & 2 * q_y * q_z + 2 * q_x * q_w & 1 - 2 * {q_x}^2 - 2 * {q_y}^2 \end{bmatrix} \quad (2)$$

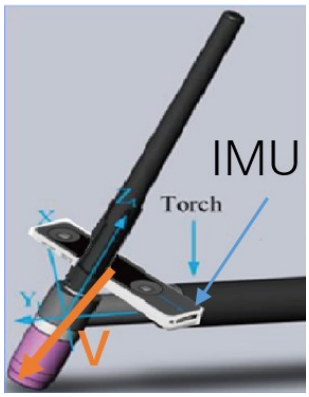

Figure 4 Correlation between sensor coordinate system and endpoint of the bypass electrode.

As V changes each time when the tungsten electrode is changed, an easy, accurate and robust approach is needed to calibrate V. To this end, we propose to touch the bypass electrode endpoint at a fixed position P_{end} after grasping the torch (after the V is fixed) and then rotate the torch. This results in, as P_{end} is fixed, with (T_j, R_j) being the jth reading from the sensor during the rotation:

$$\begin{gathered} R_1 * V + T_1 = R_2 * V + T_2 \\ R_3 * V + T_3 = R_4 * V + T_4 \\ \dots \\ R_{n-1} * V + T_{n-1} = R_n * V + T_n \end{gathered} \quad (3)$$

or

$$\begin{gathered} (R_1 - R_2) * V = T_2 - T_1 \\ (R_3 - R_4) * V = T_4 - T_3 \\ \dots \\ (R_{n-1} - R_n) * V = T_n - T_{n-1} \end{gathered} \quad (4)$$

Denote

$$X = \begin{bmatrix} R_1 - R_2 \\ R_3 - R_4 \\ \dots \\ R_{n-1} - R_n \end{bmatrix}, Y = \begin{bmatrix} T_2 - T_1 \\ T_4 - T_3 \\ \dots \\ T_n - T_{n-1} \end{bmatrix} \quad (5)$$

Then the least square estimate of V is:

$$V = (X' * X)^{-1} * X' * Y \tag{6}$$

The least square estimation allows V be accurately calibrated from relatively large number of automatically obtained sensor readings. As such, $P_{end}(k)$ can be subsequently determined from (T_k, R_k) in real-time during the operation of the human welder.

Figure 5 illustrates the trajectory of the bypass electrode's endpoint during the operation by a human welder, who positions the GTAW torch in front of the moving tractor along the X-direction. Since the tractor moves at a nearly constant speed, the human welder sustains a relatively consistent motion along the X-axis. However, we can observe gradual shifts along the Y- and Z-axes from Figure 5. These shifts are understandable, considering that the Y-axis of the IMU sensor may not be perfectly perpendicular to the tractor's moving direction and that the tractor rack may not be perfectly horizontal. Additionally, human operation introduces some fluctuations. As the trajectory of the wire endpoint P_{wire} can also be obtained from the IMU sensor installed on the tractor, their respective distance $d(k) = \|P_{wire}(k) - P_{end}(k)\|$ can be obtained as shown in Figure 6 by assuming that the wire tip maintains a constant relationship with the IMU sensor installed on the tractor. As we will only use this $d(k)$ as the first approximation, assuming a constant position of the wire tip in relation to the tractor is reasonable.

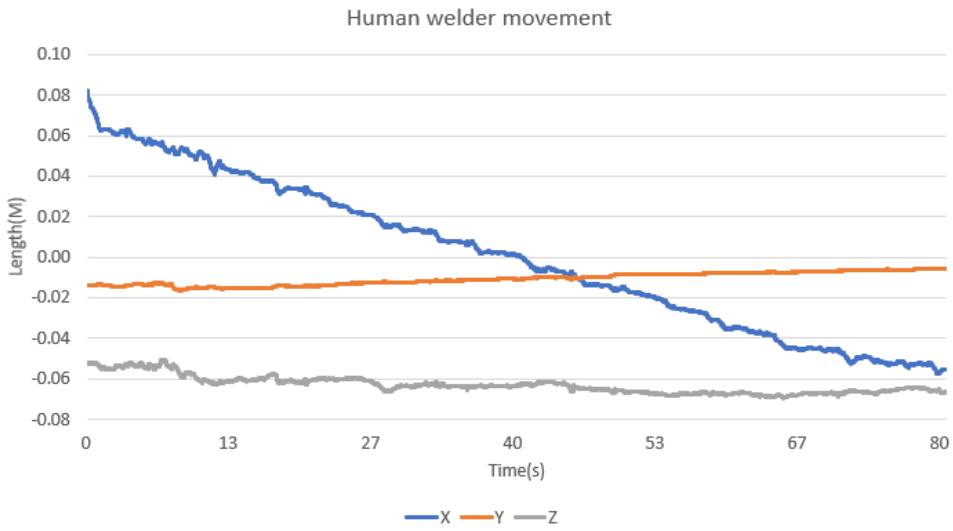

Figure 5 Trajectory of bypass electrode operated by a human welder.

The obtained distance has a fluctuation around $[-0.5mm, 0.5mm]$. Given this level of inaccuracy, relying on this distance measurement alone is insufficient to ensure precise robotic control to replace human tasks. Therefore, a more effective approach involves direct distance calculation from the captured images. Conventional methods relying on manually crafted features prove unstable during welding operations. Thus, this study proposes the utilization of a deep learning model for image processing to accurately sense the distance between the two electrodes as a human welder. Utilizing the extensive yet imprecise distance data generated by the IMU sensors, a pre-trained convolutional neural

network (CNN) will be trained, followed by fine-tuning process with a small set of manually labeled data to enhance accuracy. Figure 7(a) shows an image captured during the welding process and the definition of the distance between the electrodes. We note that we have reduced the distance from that between the two endpoints to the distance in the proceeding direction for simplification. As such, the distance hereafter is the simplified one as defined in Figure 7(a) which is actually a more reasonable one by more accurately defining/measuring the length of the bypass arc or the gap between the wire and the bypass electrode. With a precise manual labeling process, an accurate distance data pair $[d_k, I_k]$ can be obtained where d represents the distance between two electrodes and I represents the corresponding image. Figure 7(b) plots a part of manual labeled distance data. As such, we now have the datasets to pre-train and finely-train a deep learning model to calculate the distance from the arc image.

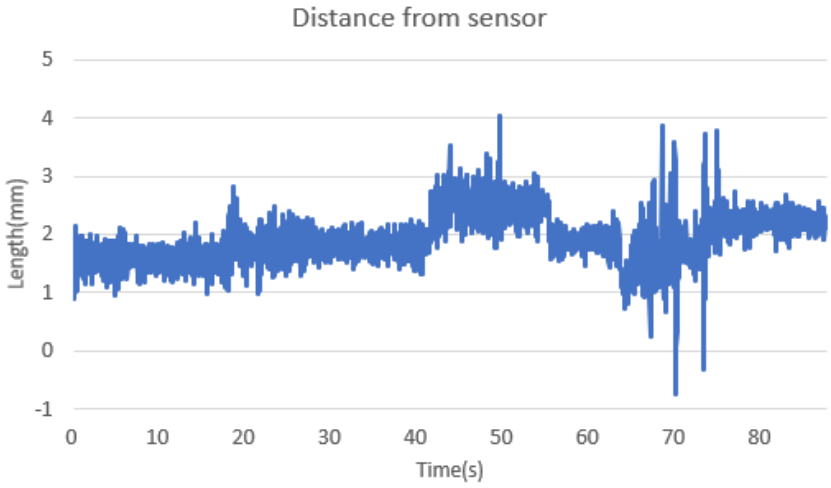

Figure 6 Distance between endpoints of the wire and bypass electrode during operation of human welder.

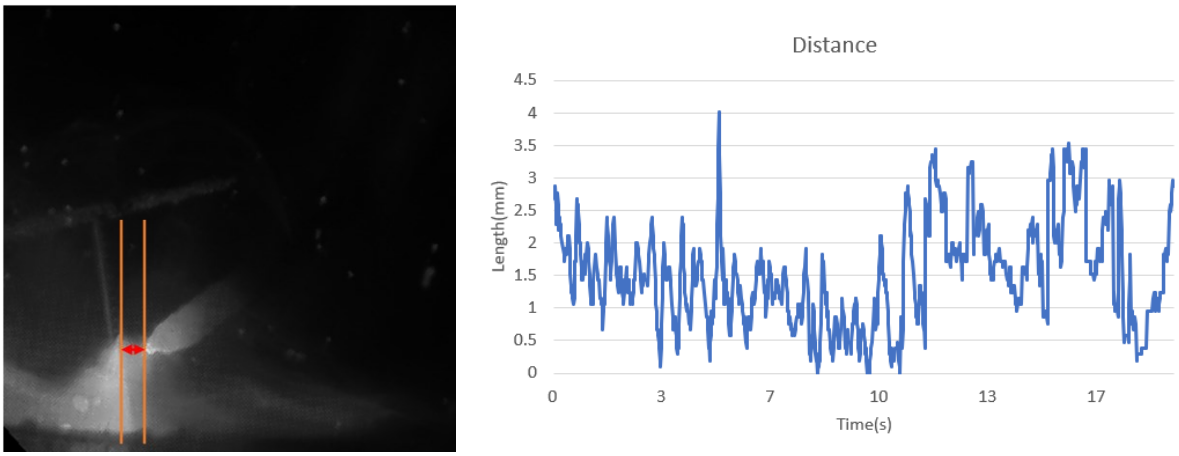

(a) (b)

Figure 7 Manually labeled data. (a) Definition of the distance. (b) Manually labeled distance.

4 Network and Training

4.1 Pre-training and fine-tuning

In this study, utilizing a 256*256 input image size, the developed model consists of 5 convolutional layers, 5 max-pooling layers, and 2 fully connected layers. Following each max-pooling layer, batch normalization and ReLU activation functions were applied. The convolutional layer parameters are (1, 16, 5, 1, 2), (16, 32, 5, 1, 2), (32, 64, 3, 2, 1), (64, 128, 3, 2, 1), and (128, 256, 3, 2, 1). The features extracted from the final max-pooling layer are flattened and fed into the initial fully connected layer comprising 256 neurons, with ReLU activation functions employed between the two fully connected layers. The second fully connected layer, consisting of 128 neurons, directly linked to the output layer without ReLU activation.

The pre-training process was conducted with an NVIDIA GTX 2080 graphics card. The model underwent 200 iterations of training with the SGD optimizer and mean square loss (MSE), utilizing the Python environment along with the PyTorch library. To ensure randomness, the dataset was shuffled during both training and validation. The training set consisted of 10,504 data pairs, while 480 data pairs were allocated for validation. The initial learning rate was set at 0.001 and decreased by 20% every 20 iterations. The training curve, depicting the loss across 200 epochs, is displayed in Figure 8(a), while the validation results are presented in Figure 8(b).

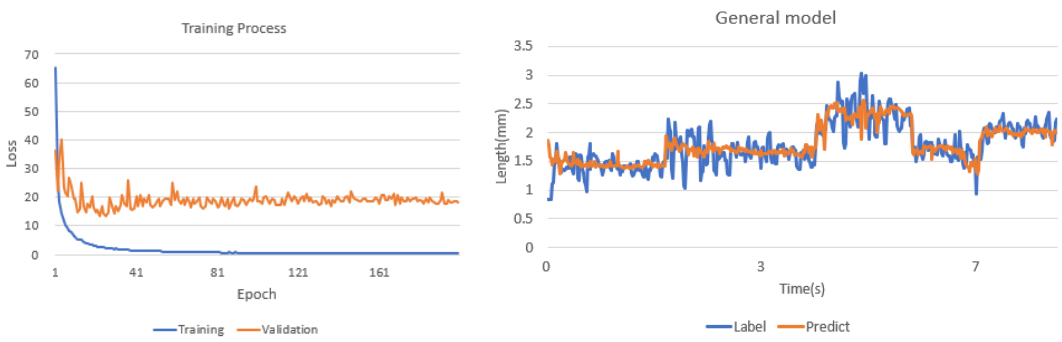

(a) (b)

Figure 8 Training curve and validation result for pre-training.

Following the pre-training phase, the model with the lowest validation loss at epoch 26 was chosen for fine-tuning. The training parameters remained consistent with the pre-training process, except for the reduction of the learning rate to 0.0001. During fine-tuning, only the last two fully connected layers were trained, while the parameters in the five convolutional layers were frozen. The training dataset comprised 1,600 data pairs, with 93 data pairs allocated for validation. The results are illustrated in Figure 9, where (a) displays the training curve and (b) presents the validation results. It is apparent that the validation results prove that the distance could be accurately sensed with the model.

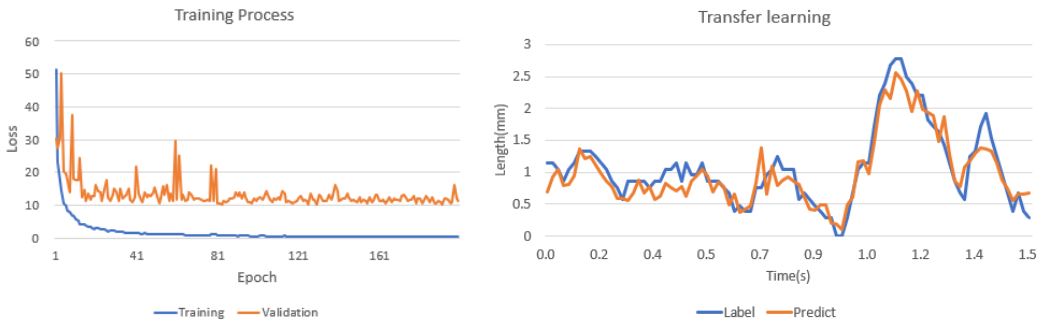

(a) (b)

Figure 9 Training curve and validation result for fine-tuning. (a) Training; (b) Validation result.

4.2 Dynamic Analysis

The images constitute the primary input for human welders and their control actions are results in response to their observed images. The mechanism through which human welders adjust their position raises the question of whether this adjustment is primarily based on the current image or a sequence of past images. In order to explore this, we train an additional CNN model that takes the current image I_k as input to predict the distance d_{k+1} in the next image. The validation outcomes are shown in Figure 10.

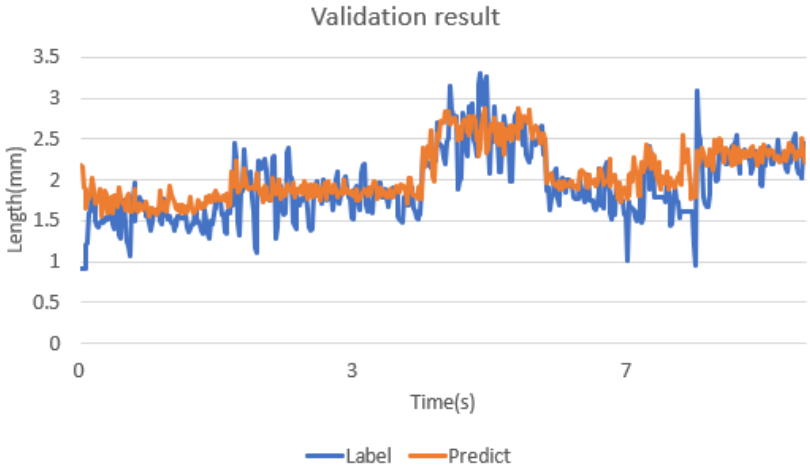

Figure 10 Validation result for the subsequent distance.

The validation illustrates that the model's outputs function as a filter on the human adjustment of position. It's apparent that human welders maintain a relatively stable distance rather than drastically altering the torch's position. However, due to the inherent constraints of human control, achieving precision and accuracy at this level remains challenging. Their behavior shows variations around the intended distance. Considering velocity information as a reference, as shown in Figure 11, reveals that velocity information contains significant fluctuations. Such fluctuations may not be intentionally made adjustments by human welders. Instead, these variations could occur from overreaction and subsequent corrective actions were taken by the welder.

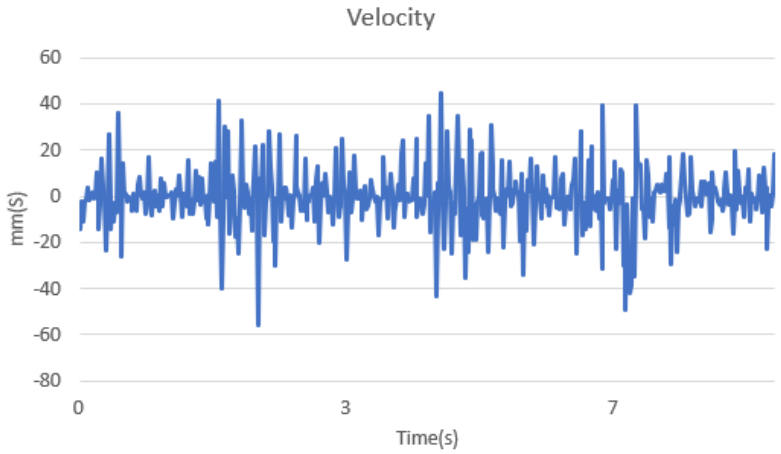

Figure 11 Human welder velocity information.

To deeply investigate the time dependency of human operation, we propose to use a CNN-LSTM (CNN long-short term memory) model illustrated in Figure 12. The CNN structure is same as the previous model while the LSTM structure has 3 layers with 256 as input size and 128 as hidden size.

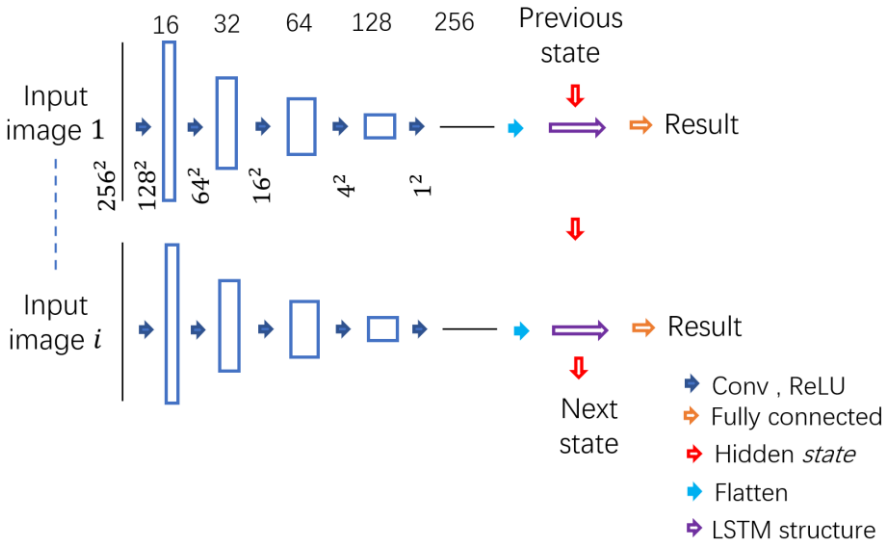

Figure 12 CNN-LSTM structure.

Utilizing the LSTM structure, the model acquires the capability to forecast the subsequent movement action based on the historical trends, i.e., deciding the next operation based on the arc state and its history. We train two models with the window set as 3 and 6, i.e., take the past 3 $I_{k-j}{}'s$ $(j = 1,2,3)$ and 6 images $I_{k-j}{}'s$ $(j = 1,2,\dots,6)$ as the input respectively to generate the current output L_k. The validation result is shown in Figure 13. Compared with the result in Figure 10, the inclusion of additional input information contributes to the smoothing of input dynamics and, subsequently, the prediction results. However, the accuracy was reduced. This outcome substantiates the notion that instant changes in the arc prompt immediate adjustments by human welders. Their decision-making process is predominantly influenced by the current state of the arc, with limited regard for its historical

states. In essence, the human welders' memory of past arc states is minimal. When a human welder takes an operation to move the torch, they already possess an estimation of the torch's final position before the control action concludes. Based on their experience, subsequent action will promptly perform to achieve their desired control operation.

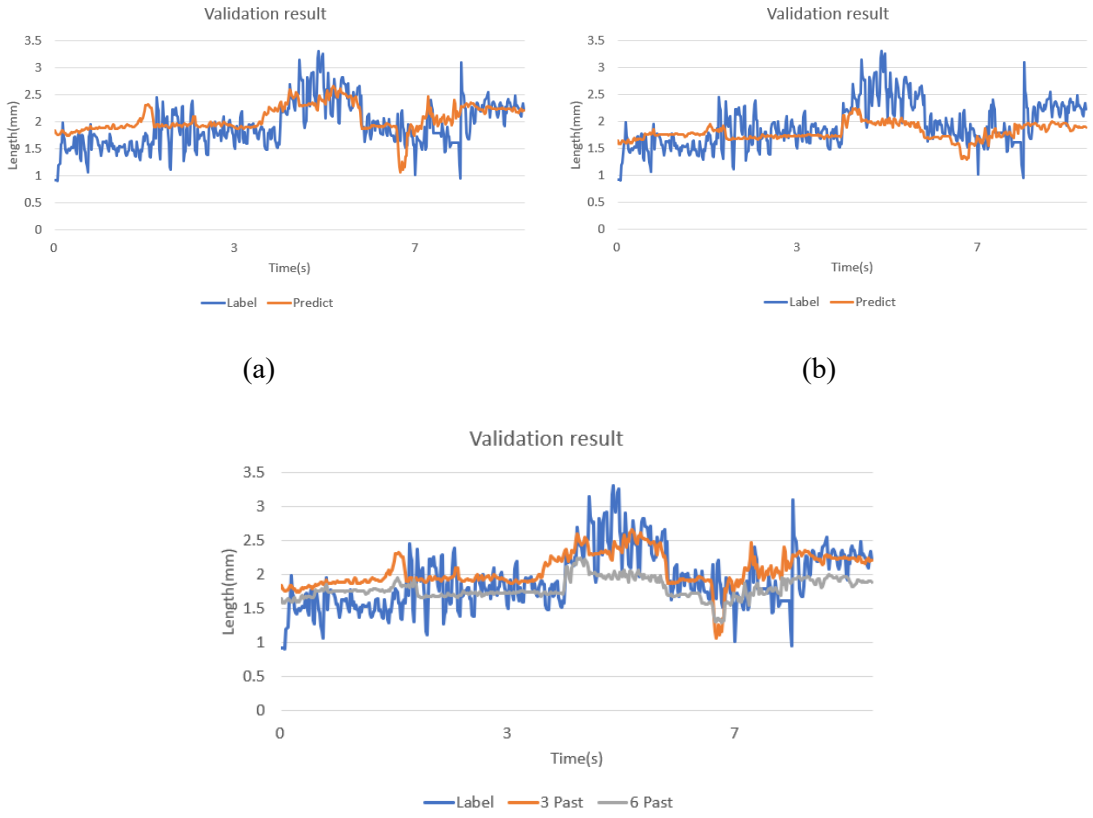

Figure 13 Validation result for using 3 past images (a) and 6 past images (b) as the input, overlapped plot for better comparison (c).

Considering the pattern in the human control information, a conclusion can be drawn that, under fixed welding parameters, experienced human welder tends to maintain a stable distance between two tips of the electrodes to sustain the bypass arc. Consequently, an optimal distance should be deduced through analyzing the distances from human experiments. Utilizing the advantage of the robot's precision, this optimal distance can be consistently maintained in the robotized DE-GMAW process, in contrast to human control.

5 Analysis of Welder Operation Behavior and Learning from Human Welder

All the arc images can be classified into three different modes. The arc images in the same mode can be used to calculate respective distances. The first mode, known as the open arc, represents the initial phase of the DE-GMAW process, where the bypass arc has yet to ignite. Under this condition, the distance between the GTAW and GMAW torches can vary. However, our primary focus lies on the subsequent two modes: parallel arc and serial arc. In these two modes, the DE-GMAW process is

underway, and the distance between the electrodes significantly affects the arc behaviors and the ability of the process to deliver the intended benefits. As shown in Figure 14, over 4140 distance data points were used to plot the histogram. When the distance is less than 2 mm, the process maintains a desired parallel arc. As the distance increases, the arc quality deteriorates rapidly, transitioning to a serial arc state only when the gap exceeds 3 mm.

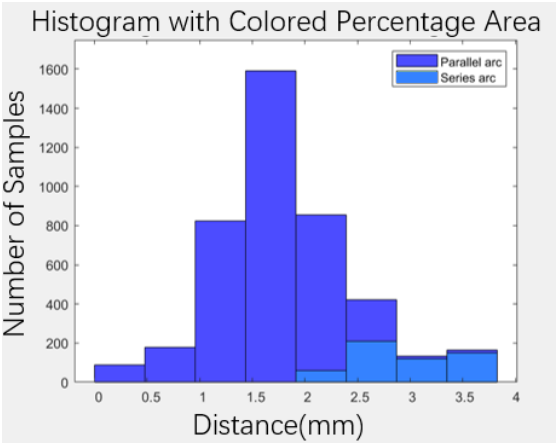

Figure 14 The percentage distribution among the DE-GMAW influenced by the endpoint distance.

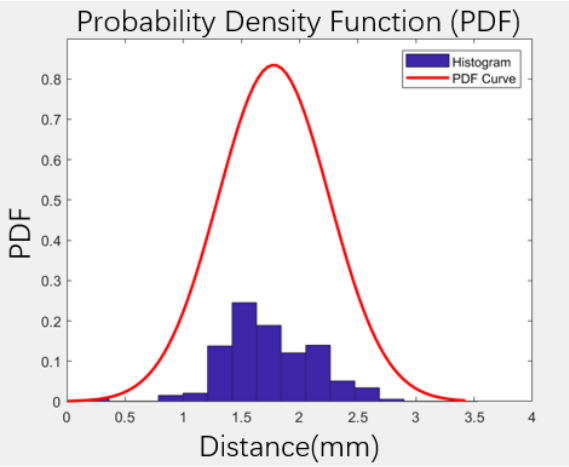

Figure 15 Probability density with the data only from desired arc mode.

Upon analyzing the data collected from the human welder operations, a distinctive pattern of adjustments emerges, marked by instances of overreactions followed by corrective actions. This pattern indicates that the quality of human welder operation is affected by human limitation. Their action cannot be as precise as a robot. The ability to accurately estimate movement is compromised; the best moving action is reached by several adjustments attempts. Therefore, the optimal welding process is achieved when the human welder minimizes torch distance adjustment, ensuring a consistently maintained gap/distance between the torches. To delve deeper into this analysis, a comprehensive exploration of distance probability is undertaken. By investigating the probability distribution of torch distances within

the dataset classified under the desired arc state as shown in the Figure 15, welding operations can be guided by maintaining the torch distance at this determined optimal value of 1.7mm.

6 Real Time Testing of Robotized DE-GMAW Process

Subsequently, the fine-tuned model was employed to process the arc image, enabling the acquisition of real-time distance feedback. Illustrated in Figure 16, a UR-10e robot was adopted to replace the human welder, collaborating with the tractor to regulate the bypass electrode. This collaboration aimed to sustain the distance at the ideal value of 1.7 mm, following the control protocol shown in Figure 17.

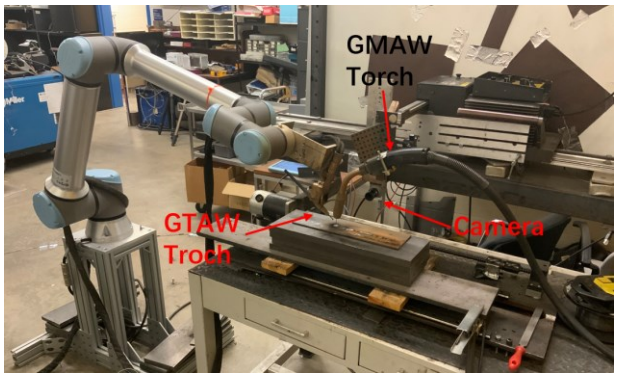

Figure 16 Robot welding experimental platform.

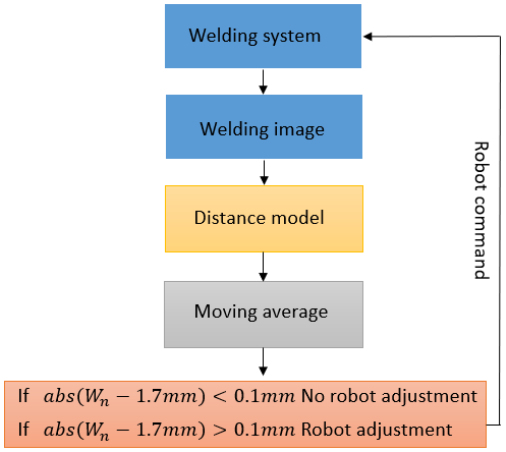

Figure 17 Control protocol.

At the start of the experiment, the distance between two electrodes was set at 1.1mm. After the process ran stably for 4 seconds, the robot intentionally moved the bypass electrode away from the wire to create a larger distance. In the meantime, the deep learning model processes the arc images to provide feedback on the changing distance. The distance from the model was filtered by moving average with window size of 20. To reduce unnecessary adjustments while still sustaining the desired mode, a 0.1 mm tolerance threshold has been set. (The resolution of the UR 10e robot is 0.05 mm.) The designed CNN model processes each image under 0.014 second, ensuring that a 60Hz sampling rate meets the requirements for fast and accurate control. During the welding process, the system was designed to sustain a constant distance (1.7 mm) between two electrodes, based on the calculated distance from the

CNN model's output. To provide visual assessment on the robotized process, the robot started to control/adjust the position of the bypass electrode 2 seconds after it was moved away. As the control algorithm identified that the gap had exceeded the desired threshold, it issued a prompt command to the robot, instructing it to execute precise movements that would restore the distance to the optimal range. This process repeats one time again after 2 seconds, with the robot intentionally shifted 0.1 cm farther than the previous shift.

Figure 18 shows the distance, where (a) is the distance calculated by $d(P_{wire} - P_{end})$ after the welding and (b) is the distance sensed by the network during the welding process. It proves that the model can successfully track the distance with smaller fluctuations than sensor.

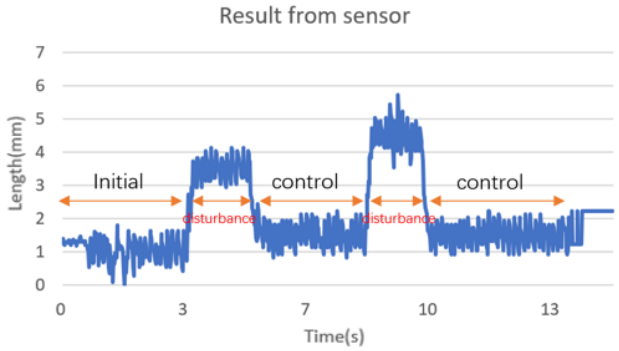

(a)

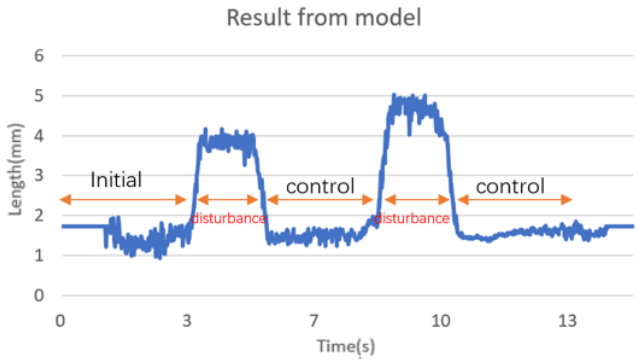

(b)

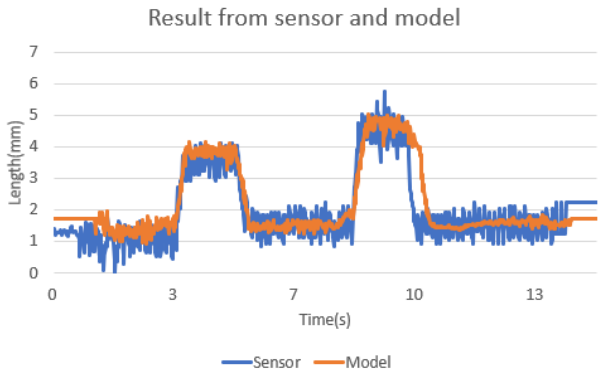

(c)

Figure 18 Distance between two electrodes during robotized DE-GMAW.

7 Conclusion and future work

The DE-GMAW process presents a method to reduce heat impact on workpieces by decoupling mass and heat input, making it particularly suitable for WAAM. However, existing efforts have utilized fixed torch relationships which limit the process adaptability. To overcome this constraint, this research suggests the robotization of this complex welding process, enhancing flexibility. This increased flexibility holds promise for advancing arc-based Additive Manufacturing techniques, thereby augmenting their automation and precision potential.

Since DE-GMAW process has not yet been robotized, this work proposes to learn from human welders. For this purpose, IMU sensors are attached to the torch and tractor, providing position data based on their respective coordinate systems. This provides data to study how human welders collaborate with the tractor. However, due to the limitation of sensor accuracies, deep learning is suggested for more accurate calculation of the distance from arc images. A CNN is pre-trained and fine-tuned for this purpose.

Examination of welder behavior uncovers overreaction patterns, indicating human limitations. Distance emerges as a pivotal factor for optimal welding outcomes. Analysis of probability distributions of electrode distances in desired arc states provides what we need to learn from human welders to robotize the DE-GMAW process. DE-GMAW has been robotized with instant torch distance feedback to consistently maintain the two electrodes at the optimum distance to deliver the desirable arc mode.

As such, this study not only sheds light on the DE-GMAW process but also pioneers its robotization. Future endeavors will contribute to refining control strategies under varying conditions, including adjustments for different voltage/current levels and adaptive manipulation of torch relationships across diverse welding scenarios.

Acknowledgment

This work is funded by the National Science Foundation under Grant No. 2024614.

Declarations

Conflict of interest: The authors declare no competing interests.

References

1. Norrish, J., 1992. Advanced welding processes. Springer Science & Business Media.
2. Cheng, Y., Yu, R., Zhou, Q., Chen, H., Yuan, W. and Zhang, Y., 2021. Real-time sensing of gas metal arc welding process–A literature review and analysis. Journal of Manufacturing Processes, 70, pp.452-469.
3. Wang X, Hua Y, Gao J, et al. Digital Twin Implementation of Autonomous Planning Arc Welding Robot System. Complex System Modeling and Simulation, 2023, 3(3): 236-251. https://doi.org/10.23919/CSMS.2023.0013

4. Henckell, P., Gierth, M., Ali, Y., Reimann, J. and Bergmann, J.P., 2020. Reduction of energy input in wire arc additive manufacturing (WAAM) with gas metal arc welding (GMAW). Materials, 13(11), p.2491.
5. Xia, C., Pan, Z., Polden, J., Li, H., Xu, Y., Chen, S. and Zhang, Y., 2020. A review on wire arc additive manufacturing: Monitoring, control and a framework of automated system. Journal of manufacturing systems, 57, pp.31-45.
6. Han, Q., Li, Y. and Zhang, G., 2018. Online control of deposited geometry of multi-layer multi-bead structure for wire and arc additive manufacturing. In Transactions on Intelligent Welding Manufacturing: Volume I No. 1 2017 (pp. 85-93). Springer Singapore.
7. Dharmendra, C., Gururaj, K., Pradeep, K.G. and Mohammadi, M., 2021. Characterization of κ-precipitates in wire-arc additive manufactured nickel aluminum bronze: A combined transmission Kikuchi diffraction and atom probe tomography study. Additive Manufacturing, 46, p.102137.
8. Chaudhari, R., Parikh, N., Khanna, S., Vora, J. and Patel, V., 2022. Effect of multi-walled structure on microstructure and mechanical properties of 1.25 Cr-1.0 Mo steel fabricated by GMAW-based WAAM using metal-cored wire. Journal of Materials Research and Technology, 21, pp.3386-3396.
9. Fang, Q., Zhao, L., Chen, C.X., Cao, Y., Song, L., Peng, Y. and Yin, F.X., 2022. 800 MPa Class HSLA Steel Block Part Fabricated by WAAM for Building Applications: Tensile Properties at Ambient and Elevated (600 C) Temperature. Advances in Materials Science and Engineering, 2022.
10. Wang, X.W., Yang, D.Q., Yong, H., Li, X.P., Lei, W., Zhang, G.J., 2021. Microstructure and Mechanical Properties of NiCrMoV Steel Fabricated by Double-Electrode Gas Metal Arc Additive Manufacturing. Journal of Materials Engineering and Performance 30, no. 9 (2021): 6656-6666.
11. Zhang, K., Xiong, J., Liu, G. and Zhang, G., 2022. Role of bypass current on pores in double-electrode gas metal arc additive manufactured 2219 aluminum alloy. The International Journal of Advanced Manufacturing Technology, 121(7-8), pp.4503-4516.
12. Liu, G., Xiong, J. and Tang, L., 2020. Microstructure and mechanical properties of 2219 aluminum alloy fabricated by double-electrode gas metal arc additive manufacturing. Additive Manufacturing, 35, p.101375.
13. Yang, D. and Zhang, G., 2017. Deposition time and thermal cycles of fabricating thin-wall steel parts by double electrode GMAW based additive manufacturing. In MATEC Web of Conferences (Vol. 88, p. 01007). EDP Sciences.
14. Yang, D., Wang, G. and Zhang, G., 2017. A comparative study of GMAW-and DE-GMAW-based additive manufacturing techniques: thermal behavior of the deposition process for thin-walled parts. The International Journal of Advanced Manufacturing Technology, 91, pp.2175-2184.
15. Trivedi, P., Vansjalia, R., Erra, S., Narayanan, S. and Nagaraju, D., 2023. A fuzzy CRITIC and fuzzy WASPAS-based integrated approach for wire arc additive manufacturing (WAAM) technique selection. Arabian Journal for Science and Engineering, 48(3), pp.3269-3288.
16. Omiyale, B.O., Olugbade, T.O., Abioye, T.E. and Farayibi, P.K., 2022. Wire arc additive manufacturing of aluminium alloys for aerospace and automotive applications: A review. Materials Science and Technology, 38(7), pp.391-408.

17. Huang, J., Yuan, W., Yu, S., Zhang, L., Yu, X. and Fan, D., 2020. Droplet transfer behavior in bypass-coupled wire arc additive manufacturing. Journal of Manufacturing Processes, 49, pp.397-412.
18. Huang, J., Guan, Z., Yu, S., Yu, X., Yuan, W., Liu, S. and Fan, D., 2021. Simulation and control of metal droplet transfer in bypass coupling wire arc additive manufacturing. The International Journal of Advanced Manufacturing Technology, 115(1-2), pp.383-395.
19. Jiang, F., Miao, Q., Xu, B., Tashiro, S., Tanaka, M., Lin, S., Fan, C. and Chen, S., 2022. Numerical analysis of physical characteristics and heat transfer decoupling behavior in bypass coupling variable polarity plasma arc. Materials, 15(9), p.3174.
20. Ma, C., Yan, Y., Yan, Z., Liu, Y., Wu, X., Li, D., Zhao, L., Liu, P. and Jin, H., 2022. Investigation of bypass-coupled double-pulsed directed energy deposition of Al–Mg alloys. Additive Manufacturing, 58, p.103058.
21. Zhang, Y.M., Li, P., Chen, Y. and Male, A.T., 2002. Automated system for welding-based rapid prototyping. Mechatronics, 12(1), pp.37-53.
22. Zhang, Y., Chen, Y., Li, P. and Male, A.T., 2003. Weld deposition-based rapid prototyping: a preliminary study. Journal of Materials Processing Technology, 135(2-3), pp.347-357.
23. Mukherjee, T., Zhang, W. and DebRoy, T., 2017. An improved prediction of residual stresses and distortion in additive manufacturing. Computational Materials Science, 126, pp.360-372.
24. Srivastava, M., Rathee, S., Tiwari, A. and Dongre, M., 2023. Wire arc additive manufacturing of metals: A review on processes, materials and their behaviour. Materials Chemistry and Physics, 294, p.126988.
25. Dutra, J.C., Silva, R.H.G.E., Savi, B.M., Marques, C. and Alarcon, O.E., 2016. New methodology for AC-pulsed GMAW parameterization applied to aluminum shipbuilding. Journal of the Brazilian Society of Mechanical Sciences and Engineering, 38, pp.99-107.
26. Panchenko, O., Kurushkin, D., Mushnikov, I., Khismatullin, A. and Popovich, A., 2020. A high-performance WAAM process for Al–Mg–Mn using controlled short-circuiting metal transfer at increased wire feed rate and increased travel speed. Materials & Design, 195, p.109040.
27. Tian, Y., Shen, J., Hu, S., Gou, J. and Cui, Y., 2021. Effects of cold metal transfer mode on the reaction layer of wire and arc additive-manufactured Ti-6Al-4V/Al-6.25 Cu dissimilar alloys. Journal of Materials Science & Technology, 74, pp.35-45.
28. Li, K.H., Chen, J.S. and Zhang, Y., 2007. Double-electrode GMAW process and control. WELDING JOURNAL-NEW YORK-, 86(8), p.231.
29. Li, K.H. and Zhang, Y.M., 2008. Consumable double-electrode GMAW-Part 1: The process. WELDING JOURNAL-NEW YORK-, 87(1), p.11.
30. Yang, D., He, C. and Zhang, G., 2016. Forming characteristics of thin-wall steel parts by double electrode GMAW based additive manufacturing. Journal of Materials Processing Technology, 227, pp.153-160.
31. Xue, C., Shi, Y., Fan, D. and Li, W.D., 2010. Edge extraction algorithm for dual bypass GMAW weld pool. Shanghai Jiaotong Daxue Xuebao/Journal of Shanghai Jiaotong University, 44(SUPPL 1), pp.4-7.

32. Liu, Y., Zhang, W. and Zhang, Y., 2013. Dynamic neuro-fuzzy-based human intelligence modeling and control in GTAW. IEEE Transactions on Automation Science and Engineering, 12(1), pp.324-335.
33. Liu, Y. and Zhang, Y., 2014. Iterative local ANFIS-based human welder intelligence modeling and control in pipe GTAW process: A data-driven approach. IEEE/ASME Transactions on Mechatronics, 20(3), pp.1079-1088.
34. Liu, Y. and Zhang, Y., 2015. Supervised learning of human welder behaviors for intelligent robotic welding. IEEE Transactions on Automation Science and Engineering 14 (3), 1532-1541
35. Yu, R., Cao, Y., Martin, J., Chiang, O. and Zhang, Y., 2023. Deep-learning based supervisory monitoring of robotized DE-GMAW process through learning from human welders. Welding in the World. https://doi.org/10.1007/s40194-023-01635-y